

Detecting rainfall interception in an Amazonian rain forest with eddy flux measurements

Matthew J. Czikowsky*, David R. Fitzjarrald

Atmospheric Sciences Research Center, University at Albany, State University of New York, United States

ARTICLE INFO

Article history:

Received 15 May 2009

Received in revised form 10 July 2009

Accepted 2 August 2009

This manuscript was handled by K. Georgakakos, Editor-in-Chief, with the assistance of V. Lakshmi, Associate Editor

Keywords:

Interception

Eddy covariance

Amazon rain forest

SUMMARY

We introduce a new method to estimate rainfall interception and demonstrate its use for data obtained in an old-growth rain forest in the eastern Amazon basin. The approach is to use eddy covariance evaporation observations to estimate the 'excess' evaporation that occurs following individual events. Ensemble averaged water vapor fluxes were calculated from original high frequency data both for rain event and for base state dry days. Interception was inferred from the difference between observed evaporation for selected times during and following rainfall events from baseline evaporation estimates. This method allows the interception evaporation to be directly measured rather than determined from the residual of incident precipitation and throughfall. In conventional studies, large differences in throughfall can occur on a site due to varying forest canopy density, structure and the appearance of canopy gaps. This problem is mitigated when using the current approach, which provides an average interception value over the flux footprint area.

Identification of light rainfall events not detected by an on-site tipping bucket rain gauge was aided by the use of a ceilometer. The mean interception for all events in the study (daytime and nocturnal) was 11.6%, comparable to some recent conventional studies in this region. We found an approximately 15% increase of evaporative fraction on the rain days as compared to dry baseline days, with the energy being supplied by a corresponding decrease in the canopy heat storage. Since net radiation is used to scale the evaporation in this method, this method may be applicable to data from other tower sites in varying surface and climatic types. We did not find that bulk stomatal resistance vanishes just after rainfall. The effective bulk stomatal resistance can be used as the observational equivalent of the wet fraction of canopy parameter used in interception models.

© 2009 Elsevier B.V. All rights reserved.

Introduction

The interception process

Interception of rainfall by the forest canopy and the subsequent evaporation into the atmosphere constitute an important part of the hydrological balance in forested regions. On an annual basis, transpiration in a forest environment is the dominant component of evapotranspiration, followed by interception evaporation and then bare-soil and litter evaporation. However, during and following transient precipitation events, re-evaporation of intercepted water exceeds transpiration as the dominant component of evapotranspiration, shifting the hydrological balance. As intercepted water evaporates, some of the leaves are wet, increasing the sto-

matal conductance to an amount depending on the fraction of wet canopy. Under such conditions, surface physiological controls are reduced, and enhanced evaporation of intercepted water can be expected from forests compared to shorter vegetation in all climatic zones (Newson and Calder, 1989). Evaporation from a wet forest canopy can exceed dry surface vegetation transpiration by a factor of five (Hewlett, 1982). During interception-loss periods with an unsaturated canopy, two-thirds of total evapotranspiration can be evaporation of intercepted water from the leaf surfaces (Stewart, 1977).

An appreciable fraction of water vapor in the Amazon is recycled through evapotranspiration, with 25–50% of Amazon precipitation having been previously evaporated from the forest (Salati and Vose, 1984; Eltahir and Bras, 1994; Hutrya et al., 2005). Lawrence et al. (2007) estimated the annual evapotranspiration partition over the Amazon to be 58% transpiration, 33% interception, and 9% soil evaporation, but the actual partition is still uncertain. Thus, the interception evaporation process is a critical part of the Amazon region water budget.

* Corresponding author. Address: Atmospheric Sciences Research Center, 251 Fuller Rd., Albany, NY 12203, United States. Tel.: +1 518 437 8743; fax: +1 518 437 8758.

E-mail address: matt@asc.cesm.albany.edu (M.J. Czikowsky).

Definitions

The surface energy balance is expressed as follows:

$$A = -(Q^* - Q_G) = Q_H + Q_E + Q_S + Q_A \quad (1)$$

where A is the available energy, Q^* the net radiation, Q_G the ground heat flux, Q_H the sensible heat flux, Q_E the latent heat flux above canopy, Q_S the biomass and air canopy storage term, and Q_A the advection term within the layer from surface to canopy top. The sign convention is upward fluxes are positive.

The surface water balance is written as follows:

$$E = P - R - \Delta S \quad (2)$$

where E is evapotranspiration, P precipitation, R runoff, and ΔS the change in soil moisture storage term. Evapotranspiration links the surface energy and water balances, expressed as Q_E in the surface energy balance and E in the surface water balance. Eq. (1) is expressed in energy units ($W m^{-2}$), but Eqs. (2)–(4) are in mass flux, or equivalent mm depth.

The components of evapotranspiration are:

$$E = E_T + E_i + E_s \quad (3)$$

where E_T is transpiration, E_i interception evaporation, and E_s the evaporation from the bare-soil and forest floor litter.

During a rainfall event over a forest, precipitation (P) either:

- falls through gaps in the canopy and reaches the ground as free throughfall (P_T), after Rutter et al. (1971);
- may be caught by leaf surfaces and then fall to the ground, contributing to the throughfall;
- may be caught by tree branches and stems and be routed down the tree trunks to the ground as stemflow (P_S); or
- may be caught by the forest canopy to be temporarily stored and then evaporated back into the atmosphere as interception evaporation (E_i).

Therefore, the forest water budget with respect to a rainfall event may be expressed:

$$P = P_T + E_i + P_S \quad (4)$$

Conventional interception-measurement methods

The most commonly-used method to estimate interception is to set up a series of rain gauges, one or more at or above the top of the forest canopy and/or in a nearby clearing to catch the total incident precipitation and numerous gauges at the forest floor to measure the precipitation reaching the ground, known as throughfall. The forest-floor rain gauges may be fixed or be periodically relocated in an attempt to improve spatial representation (so called 'roving systems'). Troughs have also been deployed at the forest floor to catch throughfall. Stemflow is collected through the use of collars placed around the tree stems and then routed into collector bins. The interception is not directly measured, but found as the residual of the total incident precipitation and the sum of throughfall and stemflow (if measured) and is usually expressed as a percentage of total precipitation. (e.g., Dingman, 2002). The measurement problem that is inherent in estimating interception evaporation in this way, particularly for tropical forests where rainfall rates are high and time for evaporation is limited, is that interception evaporation is a small difference between two large numbers, and the accumulated errors are amplified. Czikowsky (2009, p. 19) summarizes conventional methods to measure interception in tropical rain forest regions.

The models most commonly used to calculate interception at a site are the Rutter et al. (1971, 1975) numerical model and Gash's

analytical model (Gash, 1979; Gash et al., 1995). These models use the Penman-Monteith equation to calculate wet-canopy evaporation (Monteith, 1965). All require a value for the canopy storage capacity, a quantity that is commonly estimated using a linear regression of interception (or throughfall) vs. precipitation. A thorough review of interception models in use appears in Muzlylo et al. (2009).

Other methods of indirectly estimating interception include the use of a load cell-based weighing system for measuring precipitation and throughfall (Lundberg et al., 1997), use of strain gauges to measure the amount of water intercepted by individual branches (Huang et al., 2005), and the use of microwave-transmission techniques to measure canopy water storage (Bouten et al., 1991). However, these have not yet been widely used in tropical rain forests.

These conventional studies of interception in tropical rain forest sites have yielded a wide range of interception estimates, from 8% to nearly 40% of total annual precipitation (Fig. 1). Large annual interception differences can be found within plots in the same forest. Given typical heterogeneous, complex canopy and subcanopy structure and the random appearance of canopy gaps seen in tropical rain forests, conducting throughfall measurements to deploy the appropriate number and distribution of gauges to accurately sample the inherent spatial variation in throughfall to obtain a representative area-average is a major challenge. Manfroi et al. (2006) reported interception estimates ranging 3–25% in 23 subplots over a 4-ha area, the variation depending on the canopy structure and density at subplot locations. Kimmins (1973) reported that up to 100 or more rain gauges would be required to reduce the error in mean throughfall to below 5% at the 95% confidence interval. Roving rain-gauge setups help to reduce error in estimating throughfall. Deploying approximately 30–50 rain gauges over a concentrated area (such as 100 m × 100 m) and relocated weekly for a time period of a year or longer, estimated mean throughfall error has been reported to be below 5% (Lloyd and Marques, 1988; Ubarana, 1996). However, the necessary relocations are intensive and may be impractical, especially in remote locations for long observation periods.

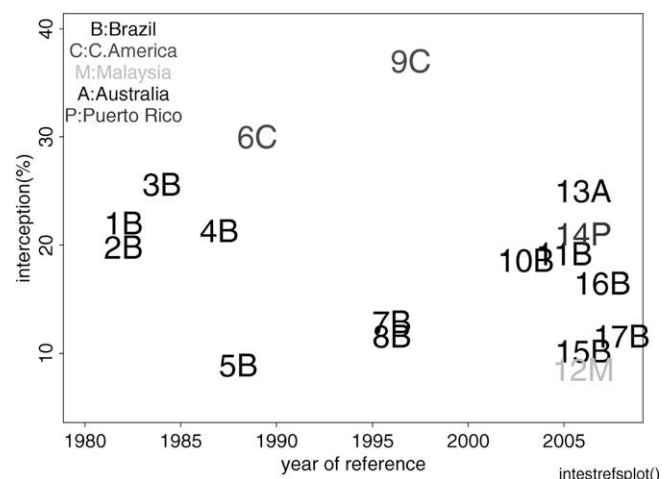


Fig. 1. Interception estimates reported in the literature using conventional methods for tropical rain forest sites. Studies done in Brazil are labeled with 'B', Central America with 'C', Malaysia with 'M', Australia with 'A', and Puerto Rico with 'P'. References are as follows: 1B, 2B: Franken et al. (1982a,b); 3B: Schubart et al. (1984); 4B: Leopoldo et al. (1987); 5B: Lloyd and Marques (1988); 6C: Imbach et al. (1989); 7B, 8B: Ubarana (1996); 9C: Cavellier et al. (1997); 10B: Arcova et al. (2003); 11B: Ferreira et al. (2005); 12M: Manfroi et al. (2006); 13A: Wallace and McJannet (2006); 14P: Holwerda et al. (2006); 15B: Germer et al. (2006); 16B: Cuartas et al. (2007). The mean interception estimate for all rainfall events in this study is denoted by 17B.

Troughs can be used to reduce the number of collectors needed to sample spatial variation in throughfall. Crockford and Richardson (1990) in a comparison of troughs to rain gauges concluded that the number of troughs deployed could be reduced by about one-fifth as opposed to the number of rain gauges to obtain the same error in mean throughfall. However, troughs also require maintenance, and suffer from splash-out and greater adhesive losses as opposed to rain gauges (Lundberg et al., 1997). Adhesive losses refer to the water collected on the trough side walls and evaporated without reaching the bottom of the trough.

A new technique for measuring interception

Through the expansion of eddy flux-measurement networks such as Fluxnet (Baldocchi et al., 2001), the number and coverage of long-term eddy flux measurement sites has grown to over 460 worldwide sites, distributed over a wide range of land cover types (<http://www.fluxnet.ornl.gov>). Interception evaporation can be inferred using eddy-covariance data already being collected.

Evaporation has been measured as the residual in the energy balance using eddy covariance (e.g., Gash et al., 1999; van der Tol et al., 2003; Cuartas et al., 2007; Herbst et al., 2008). However, this has only previously been used to derive interception evaporation under saturated canopy conditions, and not to derive total interception loss, because the method cannot separate the transpiration from the interception.

We introduce and describe a new, alternate method for observing interception using eddy-covariance data. To achieve this, we combine the eddy-covariance technique where evaporation was directly measured with novel data-analysis methods. The approach is to estimate the ‘excess’ evaporation that occurs during and following individual events, using baseline evaporation time series obtained from long time series of flux data (Fig. 2).

Rainfall over a forest perturbs the energy and hydrological budgets during and following a rain event due to interception evaporation. An advantage of using a micrometeorological approach is that one can define in time or space how the ensemble average that defines the perturbation is formed. We determine this average in the form of two *event-based ensembles*, collected from data over one forest. We associate the perturbation with the excess evaporation observed to be the result of precipitation temporarily stored in the forest canopy. The base state ensemble is composed of days without rain, corrected in such a way to exhibit approximately the same radiative conditions as rain days. The precipitation event ensemble is composed of rainy days. One assumption made is that transpiration does not stop during and following the rainfall event,

so the difference between the base state and precipitation event ensembles represents interception evaporation. This assumption is justified by our finding that bulk stomatal resistance does not vanish during and shortly after rainfall (see “Methods”).

Another advantage of this method over the traditional techniques is that interception evaporation is directly measured and not determined as net precipitation, the residual of incident precipitation and throughfall and stemflow. Furthermore, the large differences in interception that can occur on a site due to varying forest canopy density, structure and the appearance of canopy gaps is smoothed out using the eddy covariance method as the size of the flux footprint area incorporates these variations, providing an average interception value over the flux footprint area. This result provides a more suitable input for models requiring such data. Fernandes et al. (2008) state that interception estimates are not available from conventional observations on the basin scale for land-surface model comparisons. The new technique outlined in this paper could improve this situation.

Savenije (2004) argues that there is a broader definition for interception than just the difference between total precipitation and the sum of throughfall and stemflow. Interception also includes the part of the rainfall captured by the ground surface that is evaporated before it can take part in any subsequent runoff, drainage or transpiration processes. Because of this, traditional interception estimates based on net precipitation could be biased low since the wet-surface evaporation contribution to the total interception was neglected. In estimating interception using the eddy covariance method, the total evaporation is measured. Thus, both the interception evaporation contributions from the wet forest canopy and the wet ground surface are included in the eddy flux measurement.

Outline

In this paper, a new methodology for estimating interception evaporation at a site using micrometeorological measurements is introduced and described. Using the eddy-covariance technique addresses some of the shortcomings of existing interception-estimation techniques. An application of this method at an old-growth tropical rain forest site in Brazil is presented.

In “Location and data”, we introduce the study area and instrumentation used in the study. In “Identifying rainfall events, Flux calculation methods, and Flux datasets and ensemble formation”, we discuss the data-analysis methods employed, starting with rainfall-event identification methods followed by flux calculation and ensemble formation techniques. We then discuss the methods used to estimate interception during nocturnal and daytime rainfall events (“Nocturnal rainfall event methods, Individual daytime event Q_E baseline determination, and Treatment of heavy rainfall-rate periods”). We also address under what conditions micrometeorological-based interception evaporation measurements may be expected to work, and under what conditions such a technique would be of limited use. This is followed by an energy-balance comparison for dry and wet days. Finally, in “Results”, we compare our results to the conventional results reviewed in the introduction.

Location and data

The data used in this study were collected in an old-growth forest site operated as part of the Large-Scale-Biosphere-Atmosphere Experiment in Amazonia (LBA-ECO, km67 site). This site is located in the Tapajos National Forest south of Santarém, Brazil in the eastern Amazon region (2.88528°S, 54.92047°W; elevation 1170 m). The height of the forest canopy at the site is approximately 43 m.

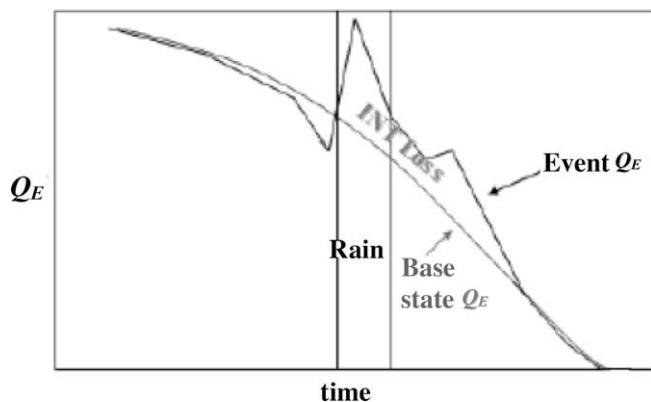


Fig. 2. Diagram illustrating the method used to estimate interception using eddy covariance. A base state ensemble Q_E is composed using dry days. The interception loss for a precipitation event is the difference between the base state and event Q_E .

An eddy-covariance system that included a Campbell CSAT3 3-D sonic anemometer (Campbell Scientific, Inc.) and a closed-path Licor 6262 CO₂/H₂O analyzer was operating at a frequency of 8 Hz at a height of 57.8 m, near the top of the flux tower at the km67 site. Net radiation was measured at 64.1 m height using a Kipp and Zonen CNR-1 net radiometer, which measured the upward and downward longwave and shortwave radiation components separately. A tipping bucket rain gauge installed at a height of 42.6 m on the tower reported precipitation at 1-min intervals with 0.1 mm resolution. A Vaisala CT-25K laser ceilometer operated at the site from April 2001 to July 2003. Along with cloud base measurements, the ceilometer provided 15-s measurements of a backscatter profile from the surface to 7500 m with 30 m vertical resolution. Cloud cover fraction was obtained by the fraction of time the ceilometer reported cloud base. The presence of forced cumulus clouds was identified by noting the proximity of the surface lifting condensation level (LCL) to cloud base. Temperature and humidity profile measurements were also taken at eight heights spanning the tower. Further site details of the flux observational system at km67 can be found in [Hutyra et al. \(2005\)](#) and [Saleska et al. \(2003\)](#). To ensure comparable timing in all instruments, eddy flux data from these collaborators was merged in real time with our own radiative flux and ceilometer data.

A large number of precipitation events need to be analyzed under similar conditions to form sufficient ensembles for this approach to work. One advantage of using this approach to estimate interception at this site is the tropical regularity in the diurnal patterns of precipitation and cloudiness, especially in the dry season. Precipitation frequently occurs during the same times of the day, helping to build an adequate ensemble of similar cases in a relatively short period. At the km67 site there is an afternoon convective peak in rainfall in both the dry and wet seasons, and a nocturnal synoptic peak in the wet season ([Fig. 3](#); [Fitzjarrald et al., 2008](#)). This regularity is evidenced by the fact that boundary layer cumulus clouds regularly form during the dry season in late morning and dissipate after nightfall ([Figs. 4 and 5](#)). This allows us to form a large ensemble of dry-day latent heat flux within a relatively short overall observation period. Furthermore, there is little day-to-day variation in cloud fraction and cloud base, especially during the dry season ([Figs. 4 and 5](#)).

Methods

Identifying rainfall events

Precipitation events were identified both using the rain gauge and from the ceilometer backscatter profile ([Fig. 6](#)). The length of the storm separation time should be long enough that the precipitation event has finished and the canopy has had ample time to dry, but not so long as to combine the rainfall of two separate events. This is important because a rainfall event is often composed of many irregularly spaced rainfall tips, each tip being the amount required to activate a counter on the rain gauge (0.1 mm in this study). A 4 h storm separation time was chosen to ensure a clear start and end time for each rainfall event. This value was

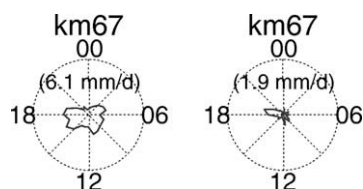


Fig. 3. Rain dials for the km67 site during the wet season (left) and dry season (right). Times listed on the rain dials are in GMT (LT + 4 h) ([Fitzjarrald et al., 2008](#)).

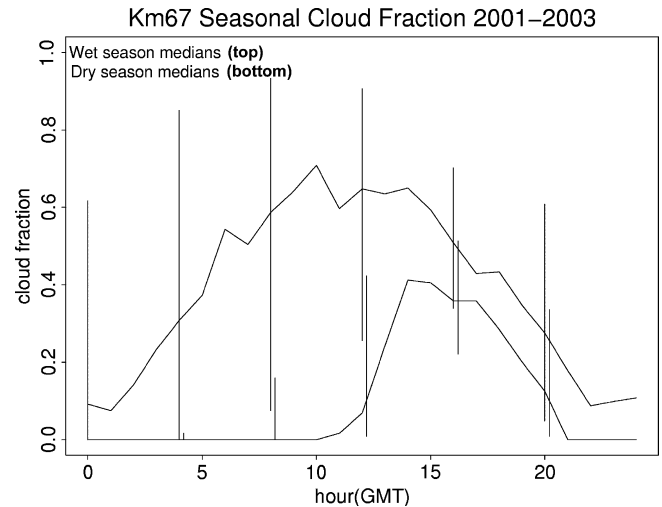


Fig. 4. Median cloud cover fraction at km67 measured by the ceilometer by hour of day for the wet season (February–May, top) and the dry season (September–December, bottom) for 2001–2003. The quartiles are indicated by the bars. Note the presence of convective cloudiness during the day in the dry season and the absence of clouds at night in the dry season. Cloud cover fraction peaks during the morning in the wet season.

successfully used by [Wallace and McJannet \(2006\)](#) in an Australian rain forest and [Van Dijk et al. \(2005\)](#) in a West Javan rain forest. This separation time worked well at this site given the regularity of the daily timing of the precipitation at this site.

From the 1-min precipitation data from the rain gauge, a precipitation event was identified in the following manner. The precipitation file was scanned until the first tip was found, the rain event start time. The rain event end time was defined as the time last tip, after which there were no further tips for the following 4 h. This process was repeated for all rain events.

Ceilometers have been used to observe boundary-layer aerosols ([Zephoris et al., 2005](#)) and detect rain droplets ([Rogers et al., 1997](#)). For convenience, we averaged the raw 15-s ceilometer data to 5-min to perform the rain-identification analysis. This had little impact on the event fluxes calculated later since the minimum flux-calculation length used was 15-min.

The same storm separation time and scanning method were used with the ceilometer data as with the rain gauge data. Two additional variables needed were a threshold value to classify precipitation, and the heights through which to average the backscatter profile. An example of ceilometer backscatter data with the range of rain-identification thresholds and rain gauge data is shown in [Fig. 7](#). Based on the review of many rainy days, the rain-identification threshold was taken as 1.2–1.5 backscatter units ($\log(10,000 \text{ srad km}^{-1})$). The largest decrease in the number of observed backscatter intensities between 1.2 and 1.3 (not shown), and a rain threshold value of 1.3 units was chosen. This choice led to event definitions that agreed well with results from visual inspection of rainfall events in the ceilometer records.

The range of backscatter profile heights to average was examined to ensure backscatter returns from clouds were not included in the rainfall-identification process. Averaging the backscatter profile up to 50% of the cloud base height yielded the best results when compared to events recorded simultaneously by the rain gauge.

One advantage of using the both the ceilometer backscatter data and rain gauge to identify precipitation events over the rain gauge alone is that ceilometer detects all rainfall events, including light ones for which the rain gauge may not catch any rainfall or not enough to force a tip. Second, the ceilometer gives the

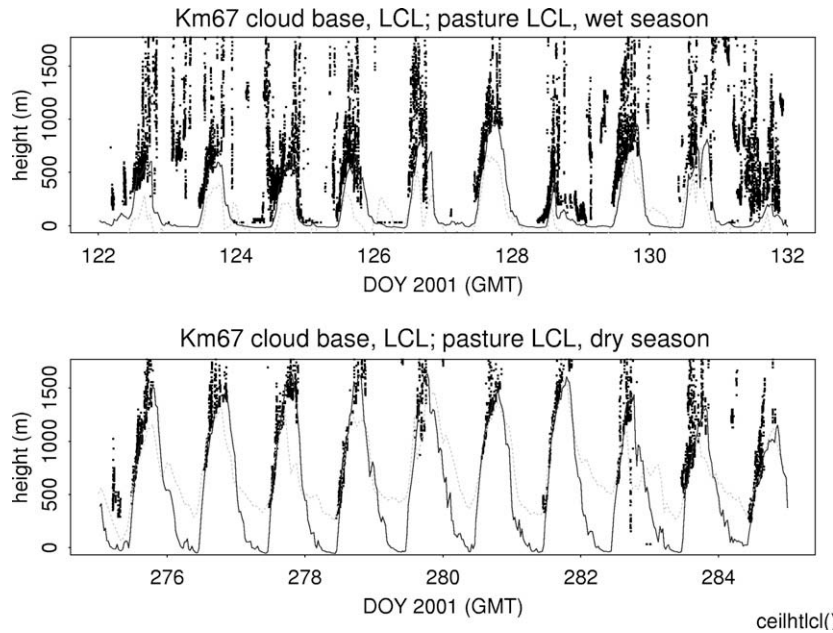


Fig. 5. Top panel: Cloud base at km67 (black dots), lifting condensation level (LCL) at km67 (gray dashed line), and LCL at km77 (solid line) during a wet season period in 2001 (May 2–11, days 122–131). Bottom panel: As in top panel but for a dry season period in 2001 (October 2–12, days 275–285).

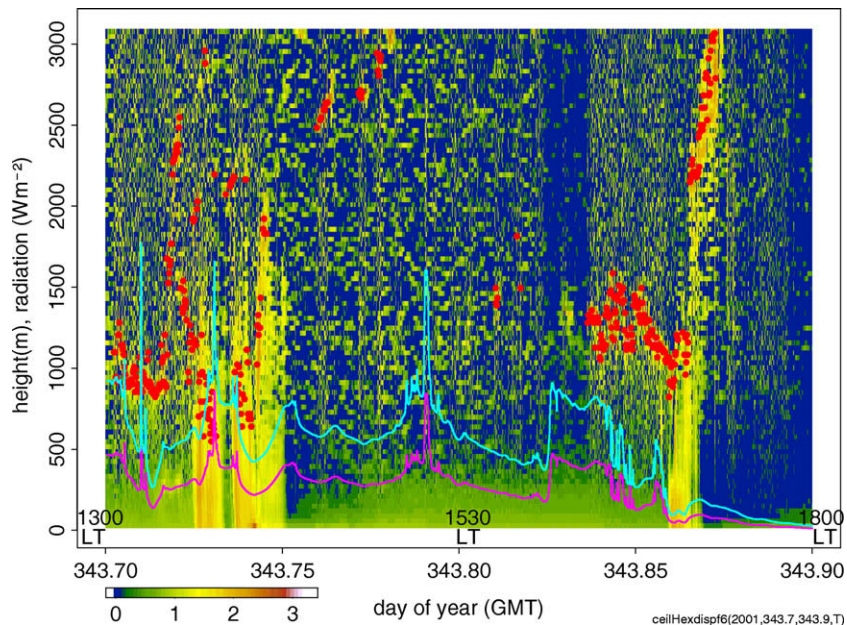


Fig. 6. Raw ceilometer backscatter (15-s samples) from 1300 to 1800 LT on December 10, 2001 at the LBA km67 site. Backscatter units are $\log(10,000 \text{ srad km}^{-2})^{-1}$. Red dots indicate cloud bases (m). The pink line is the incoming shortwave radiation (S_{down} , units of W m^{-2}). The light blue line is the photosynthetically active radiation (PARdown, units of $\mu\text{mol m}^{-2} \text{s}^{-1}$). Precipitation fell during two periods. The first event occurred in the early afternoon from 1325 to 1400 LT. A second, lighter rain shower occurred for a brief period from 1640 to 1655 LT. The on-site rain-gauge recorded 0.76 mm of precipitation for the first rain event, but none for the second rainfall. (For interpretation of the references to colour in this figure legend, the reader is referred to the web version of this article.)

instantaneous start time for rainfall, whereas with the tipping bucket rain gauge, light precipitation may have been falling for several minutes before a tip is recorded.

A total of over 200 events were identified using the tipping bucket rain gauge over the April 2001–July 2003 time period (Table 1). The on-site ceilometer detected nearly 40 light precipitation cases in the dry season that were not detected by the tipping bucket rain gauge.

Flux calculation methods

The latent heat flux Q_E and the sensible heat flux Q_H were directly measured by the eddy covariance method using the following:

$$Q_E = \overline{\rho L_v w' q'} \quad (5)$$

$$Q_H = \overline{\rho C_p w' T'} \quad (6)$$

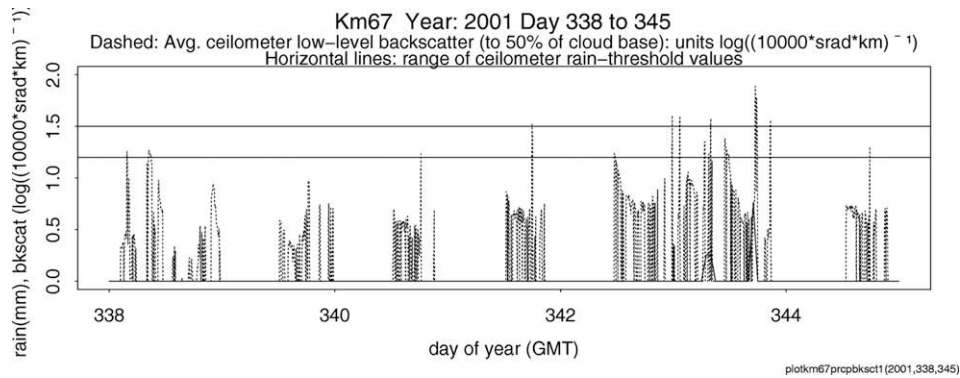


Fig. 7. Rainfall (mm, solid line at bottom), and average ceilometer backscatter up to half of the cloud base height (units of $\log(10,000 \text{ srad km}^{-1})$, dashed line) for days 338–345 in 2001. The horizontal solid lines indicate the range of rain-identification threshold values used for the ceilometer backscatter data.

Table 1

Seasonal frequency of events from available data. The wet season is defined as the months January–June, the dry season July–December. Both daytime and nocturnal events are included.

	Wet	Dry	All
Tipping bucket (2001–2003)	143	63	206
Ceilometer (2001–2002)	80	102	182

where L_v is the latent heat of vaporization, C_p the specific heat of air, and ρ the air density; \overline{wq} and \overline{wT} are the latent and sensible kinematic heat fluxes, and the overbars indicate Reynolds averaging. In the Reynolds averaging procedure, the variables to be averaged are separated into mean and turbulent components (denoted by the primed variables in Eqs. (5) and (6)) following a set of rules (e.g., Kaimal and Finnigan, 1994).

Four mean-removal methods were initially employed to make the Reynolds average for the eddy flux calculation: block-average, linear trend removal, centered running mean removal, and smoothed mean removal. Procedures for performing these mean-removal methods are found in e.g., Kaimal and Finnigan (1994). These methods have been used in standard practice in the flux measurement community, including over flux tower-measurement networks such as AmeriFlux (e.g., Massman and Lee, 2002). The block-average, linear trend, and centered running mean removal calculations follow that of Sakai et al. (2001) (see also Kaimal and Finnigan, 1994). The smoothed mean removal employed here uses a locally-weighted regression smoothing function, run in the Splus software package as the function *supsmu* (Mathsoft, Inc.; function details given in Fitzjarrald et al., 2001) to detrend the time series.

Raw data points that were recorded during calibration cycles, data points out of range for the sonic anemometer, and points with missing data were flagged. Any flux-calculation period with >2% of its raw data points flagged was discarded from the analysis.

To date there are no published studies evaluating the performance of the CSAT3 anemometer during rainfall. However, the treatment of our dataset compared to other studies using sonic anemometers during rainfall gives us confidence that our measurements are valid. First, during events with light-to-moderate rainfall rates, we did not observe fluctuating shifts in the sonic mean temperature (e.g., Mizutani et al., 1997, Fig. 4) during individual flux-calculation periods. Second, we filtered out spikes caused by raindrops striking the sonic transducer in a similar manner to Aylor and Ducharme (1995), which in their dataset comprised 0.1–0.2% of the data points during rainfall rates of 7.2 mm h^{-1} or less. Following spike removal, their turbulence statistics calculated during rainfall were in good agreement with those statistics computed during dry conditions. The failure of the method in this study at

high-rainfall rates is a result of sonic failure, when the amount of raindrop-induced spikes is larger in a given flux-calculation period.

The sensible and latent heat fluxes ultimately used in the analysis are the average of the smoothed mean removal, linear trend removal, and running mean-removal methods. The block-averaged method was very sensitive to flagged points in the data, while the other three methods were not.

Fluxes were initially calculated at 15-min and 30-min intervals. The 15-min fluxes were used for further analysis for two reasons. We found that the 30-min fluxes are insufficient to fully resolve event detail, given the transient nature of the evaporation pulses that occur during a precipitation event. Also, the use of a 30-min averaging window for the fluxes resulted in larger quantities of acceptable data being discarded surrounding regular calibration periods.

For each 15-min period the friction velocity u^* was calculated along with the mean and standard deviations of the net radiation $-Q^*$, wind speed, temperature, and humidity. The biomass and canopy air storage term Q_5 in the energy balance was calculated following the empirical relation of Moore and Fisch (1986) developed in a similar rain forest setting in Manaus, Brazil. The same relation was also used by da Rocha et al. (2004) at a rain forest site (km83 site of LBA-ECO) near the location of this study. The Q_5 term was calculated as:

$$Q_5 = 16.7\Delta T_r + 28.0\Delta q_r + 12.6\Delta T_r^* \quad (7)$$

where ΔT_r is the hourly air temperature change (C), Δq_r the hourly specific humidity change (g/kg), and ΔT_r^* is the 1 h lagged hourly air temperature change (C).

Flux datasets and ensemble formation

Taking advantage of the regularity of dry-day weather conditions in this region, we define the composition of the ensemble average in terms of an event-based ensemble, based on whether or not precipitation fell on a given day. Days without rainfall and with sufficient data were composed to form an ensemble average representing the “base state” or baseline latent heat flux; the evapotranspiration that would have occurred had precipitation not fallen (Fig. 2). Likewise, ensemble averages were formed using days with rainfall at any time of day and afternoon rainfall (to separate afternoon convective precipitation from nocturnal squall-line-associated rainfall) to represent the baseline latent heat flux for those days.

The effect of wet-canopy transpiration on the base state latent heat flux is minimal, since the evapotranspiration from wet-canopy surfaces is several times than the transpiration alone (Larsson, 1981, and references therein).

To facilitate the composition of these ensembles, two flux datasets were created, each using different sets of starting and ending times for the flux-calculation periods. In the first dataset, fluxes were calculated for consecutive 15-min periods for the entire dataset, with the first calculation period of each day beginning at midnight, regardless of the occurrence of precipitation events. This flux dataset was used in the composition of the dry-day, rain-day, afternoon rain-day baseline ensembles. The dry-day baseline ensembles for Q_E and $-Q^*$ are shown (Fig. 8).

In the second dataset, fluxes were calculated relative to the timing of each precipitation event. The starting flux-calculation time $t = 0$ for a given precipitation event depended on the manner which the event was detected. For rain-gauge-recorded events, $t = 0$ was the time of the first recorded tip by the tipping bucket rain gauge. For ceilometer-detected events, $t = 0$ was the time of the first ceilometer backscatter return detected that was beyond the threshold backscatter value. For events detected by both the rain gauge and the ceilometer, the rain gauge event times were used. Fluxes were calculated at consecutive 15-min intervals for each event starting 4 h before the start of the event until 4 h after the end of the event, which was defined as the time of the last recorded tip by the rain gauge or the last detected above-threshold ceilometer backscatter return. The precipitation event flux ensembles described below were calculated using this dataset.

Nocturnal rainfall event methods

For nocturnal cases, the situation is simpler because the base state Q_E is nearly zero at night (Fig. 9). Therefore, the nocturnal portion of event Q_E can be integrated directly and converted to an equivalent water depth. The remaining amount of water stored in the canopy that does not get evaporated the night of the event evaporates the following morning, and this portion must be addressed separately.

The individual event departures from the base state Q_E (the interception losses) were used to form an ensemble average of interception evaporation occurring during nocturnal rainfall events with respect to the starting time of each rain event.

Individual daytime event Q_E baseline determination

For daytime events, the process of determining the interception evaporation is more complex because the base state Q_E is not zero during the daytime (Fig. 2).

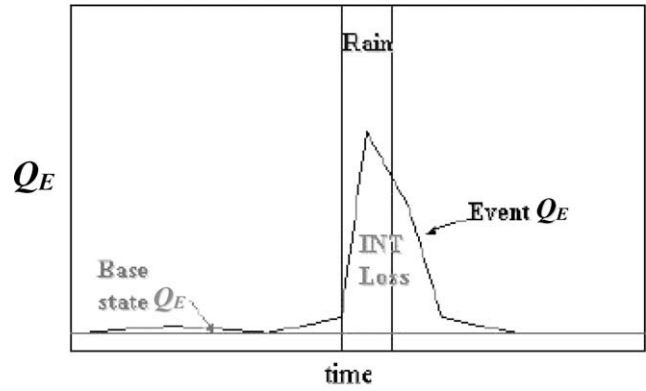


Fig. 9. Diagram illustrating the method used to determine nocturnal interception losses.

To determine the baseline dry-day Q_E for an individual rainfall event, the net radiation must be taken into account. The net radiation for a given rainfall event is less than what would be observed on a dry day at the same time of day (Fig. 10). The dry-day baseline Q_E should represent the latent heat flux that would occur on a dry day under the same radiative conditions as a day with rain. The method outlined below was used to determine the dry-day baseline Q_E . The method starts with the ensemble Q_E for all dry days ($[Q_E]_{dry}$). The brackets indicate the ensemble average was taken.

We divide the mean of the event net radiative flux ($-Q_{ev}^*$) by the mean of the dry-day baseline value ($[-Q^*]_{dry}$) for the time of day of the precipitation event to get the radiative fraction ($-Q_{frac}^*$) for the corresponding time of day covering the precipitation event. This event radiative fraction is multiplied by the raw dry-day baseline latent heat flux ($[Q_E]_{dry}$) for the same time of day to get the baseline Q_E :

$$-Q_{frac}^* = \left(\sum (-Q_{ev}^*) / n_{ev} \right) / \left(\sum ([-Q^*]_{dry}) / n_{dry} \right) \tag{8}$$

$$[Q_E]_{baseline} = -Q_{frac}^* * [Q_E]_{dry} \tag{9}$$

Details of alternate methods tested to determine the Q_E baseline for daytime events are discussed in Czikowsky (2009).

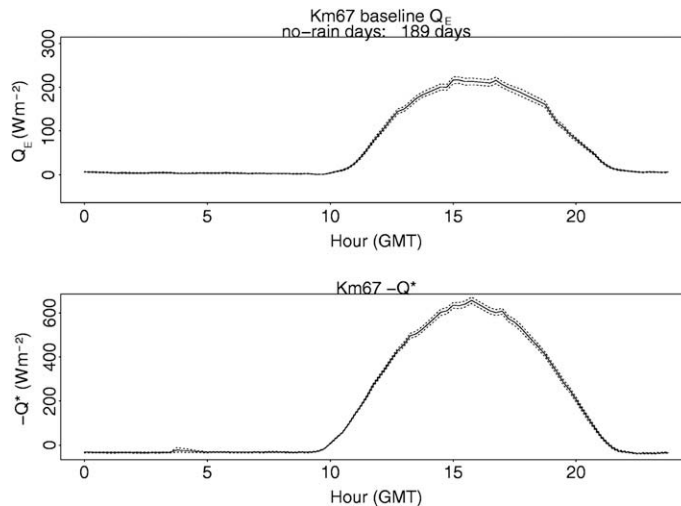


Fig. 8. (Top) Km67 ensemble mean Q_E for dry days. (Bottom): Km67 ensemble mean $-Q^*$ for dry days. The standard errors are dashed. The number of days included in the ensemble is 189.

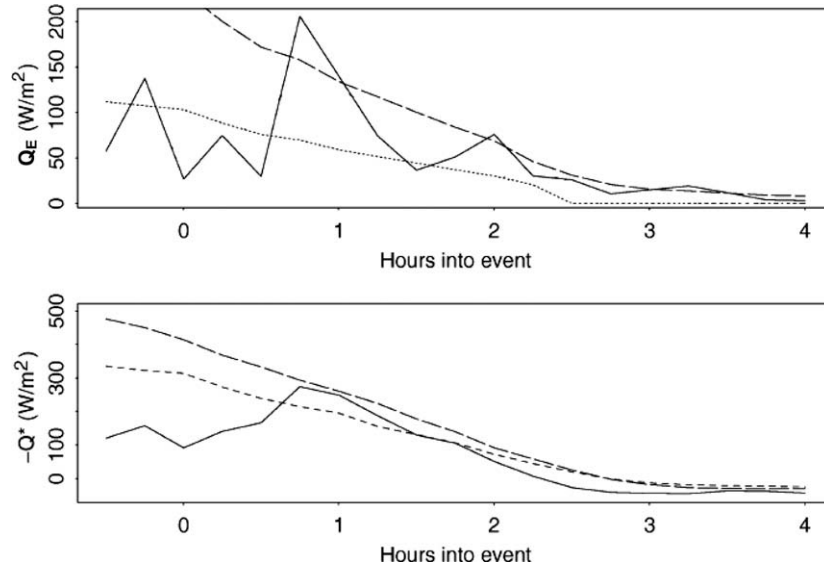


Fig. 10. Top: Precipitation event Q_E (W m^{-2} , solid line), dry-day ensemble Q_E (long dashed line), corrected dry-day baseline Q_E using method 1 (alternating dashed and dotted line), method 2 (short dashed line), and method 3 (dotted line). Bottom: Precipitation event $-Q^*$ (W m^{-2} , solid line), dry-day ensemble $-Q^*$ (long dashed line), and rain-day ensemble $-Q^*$ (short dashed line).

Treatment of heavy rainfall-rate periods

During periods of heavy rainfall, the sensors used in the eddy-covariance system may fail and therefore directly-measured latent heat fluxes cannot be obtained (e.g., Mizutani et al., 1997). Therefore, during these periods, we use the Penman-Monteith equation to estimate event latent heat flux (Monteith, 1965):

$$Q_E = \frac{\varepsilon A + \frac{\rho L_v \delta}{r'_a}}{\varepsilon + 1 + \frac{r'_s}{r'_a}} \quad (10)$$

where ε is the $L_v S_v / C_p$; where S_v is the slope of saturated specific humidity with temperature, δ the saturation deficit, and r'_s, r'_a is the stomatal, aerodynamic resistances.

The available energy was determined directly from the radiation measurements near the tower top, and temperature, humidity measurements near the tower top for the saturation deficit. The aerodynamic resistance was calculated using the following relation (e.g., Rutter et al., 1971, 1975; Mizutani and Ikeda, 1994; Wallace and McJannet, 2006):

$$r'_a = \frac{1}{k^2 u(z)} \left(\ln \frac{z-d}{z_0} \right)^2 \quad (11)$$

where z is the anemometer height, z_0 the roughness length, d the displacement height, $u(z)$ the wind speed at height z , and k is the von Karman constant.

In this study $z = 58$ m, the height of the top-level wind speed measurement. Following Monteith and Unsworth (1990), the displacement height was taken to be $0.75h$, and the roughness length equal to $0.1h$, with h being the canopy height (43 m).

Typical values for stomatal resistance used over forests are 150 s m^{-1} for dry conditions and 0 s m^{-1} for wet-canopy conditions (e.g., Raupach and Finnigan, 1988). However, using a vanishing stomatal resistance during and following rain events with our data in the Penman-Monteith calculation resulted in latent heat fluxes approximately three times the observed events when eddy-covariance data were available. At the km67 study site, ensemble stomatal resistances found as a residual term in the Penman-Monteith equation shows that on rain days, the stomatal resistance was not 0, but approximated 40 s m^{-1} during rainfall

periods. This stomatal resistance yielded much better agreement with observed Q_E during light and moderate rainfall-rate events, and we used the same value for the heavy rain-rate cases. On dry days, afternoon stomatal resistance exceeded 100 s m^{-1} at the study site.

The stomatal resistance observations at the km67 study site indicate that the full canopy is not wetted during these rain events. Lloyd et al. (1988) explain that in using the Rutter et al. (1971, 1975) model, evaporation from a saturated canopy is calculated from the Penman-Monteith equation with the stomatal resistance set to zero. However, when the depth of water stored on the canopy C is less than the canopy storage capacity S , partially wet canopy, evaporation is reduced in proportion to C/S . Imposing a stomatal resistance comparable to ensemble observations in a uniform-canopy scheme has a similar impact on the resulting evaporative flux as scaling back zero-stomatal-resistance Penman-Monteith evaporation by the fraction of the canopy that is wet.

The wet fraction of canopy F_W can be inferred directly from measurements using the ensemble bulk stomatal resistances found during dry and rain events (r'_{sd} and r'_{sr} , respectively). Assuming a fully wet canopy has zero resistance, the fraction of wet canopy can be written as:

$$F_W = \frac{[r'_{sr}]}{[r'_{sd}]} \quad (12)$$

where the brackets indicate the ensemble average was taken.

Using the ensemble bulk stomatal resistances found during dry and rain events (100 s m^{-1} and 40 s m^{-1} , respectively), we arrive at a F_W value of 40%. This value is comparable to the wet fraction of canopy that would result from considering C/S . For a study in a Bornean rainforest environment with similar interception as this study, the canopy storage capacity S was calculated as between 0.65 and 0.7 mm using both conventional (net rainfall vs. total rainfall relationship) and sapflow measurements (Kume et al., 2008; Manfroi et al., 2006). If for the depth of water on canopy C , we use the mean amount of water evaporated during the heavy rainfall events in our study (0.32 mm), then the C/S value falls between about 45% and 50%, comparable to what we found directly from the ensemble bulk stomatal resistances.

Table 2

Mean interception estimates for daytime rainfall events classed by rainfall rate. The events in the ≤ 2 mm h⁻¹ and 2–16 mm h⁻¹ rate categories used observed Q_E , whereas the event Q_E in the >16 mm h⁻¹ was filled with Penman-Monteith Q_E .

Rainfall rate (mm h ⁻¹)	Mean interception (standard error) (%)	Number of events
≤ 2	18.0 (12.2)	46
2–16	9.9 (2.6)	58
>16	7.8 (1.6)	25

Table 3

Mean interception estimates for Penman-Monteith-filled daytime rainfall events classed by rainfall rate.

Rainfall rate (mm h ⁻¹)	Mean interception (standard error) (%)	Number of events
≤ 2	21.5 (12.2)	46
2–16	14.7 (3.5)	58
>16	7.8 (1.6)	25

In tropical forests, stomata are found only on the underside of leaves in over 95% of species (Grubb, 1977; Table 3). Therefore, the assumption that water covers the stomatal openings is probably not valid for tropical forest plants with big, flat horizontal leaves. This would suggest that some transpiration is occurring during typical rainfall events, and the stomatal resistance greater than zero.

Making valid estimates of net radiation during rainfall is another issue to consider. Water droplets that collect on the net radiometer dome and decrease measured net radiation. Brotzge and Duchon (2000) show examples of a net radiation decrease of approximately 25 W m⁻² during rainfall by the Kipp & Zonen CNR-1 net radiometer used in this study, the smallest decrease among radiometers surveyed. Over the range of meteorological conditions experienced at the km67 site, this 25 W m⁻² decrease in available energy results in a 2–5% decrease in latent heat flux estimated by the Penman-Monteith equation.

Results

Nocturnal precipitation events

For the nocturnal precipitation events, ensemble means of the latent heat flux based on the rain start time show a pulse of interception evaporation starting as the precipitation begins to wet the forest canopy, even before the first recorded tip at $t = 0$ of the rain events (Fig. 11).

The nocturnal interception evaporation pulse continues for about 2 h following the event start, decreasing in magnitude with time. In the 2 h following the precipitation event start, the mean interception estimate was just under 5% of the total precipitation. Then, the evaporation pulse stopped, possibly due to the air near the ground stabilizing as a result of the nocturnal interception evaporation.

Approximately 15% of nocturnal rainfall events surveyed were associated with interception estimates $>15\%$. These high-interception nocturnal events are broken into two categories. First, there were high-interception, high-wind events occurring between 2300 LT and 0100 LT, consistent with the timing of nocturnal squall lines arriving at the site. Ensemble mean wind speeds for these events reached nearly 5 m s⁻¹. The second type of high-interception nocturnal event is a high-interception, low-wind event that occurs near the time of evening transition (≈ 1800 LT). Wind speeds during these events remained below 3 m s⁻¹ (see Czikowsky, 2009 for details).

In the early morning following a nocturnal rainfall, the remaining water stored in the canopy will be evaporated. The ensemble departure from baseline latent heat flux for the mornings after nocturnal rainfall events show a pulse of evaporation starting at about 1 h after sunrise, peaking between 2 and 3 h after sunrise at about 60 W m⁻² (Fig. 12). This evaporation pulse amounts to an additional mean amount of 0.05 mm of water evaporated during the early morning, with a standard error of 0.02 mm. Therefore, the combined mean (\pm standard error) interception for all nocturnal rainfall events is 7.2% ($\pm 1.0\%$).

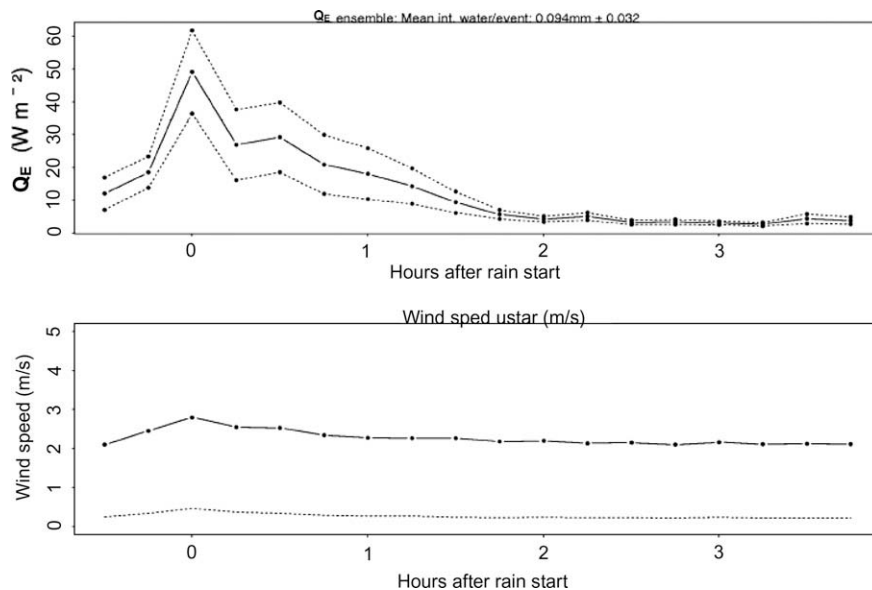


Fig. 11. Top panel: Ensemble mean latent heat flux (W m⁻²) for all 54 nocturnal precipitation events. Dotted lines indicate the standard error. The time axis refers to the number of hours before/after the first rain tip. Bottom panel: Mean wind speed (m s⁻¹, solid line) and u^* (m s⁻¹, dotted line) for the same 54 nocturnal precipitation events. The mean interception (\pm standard error) for these events is 4.7% \pm 0.9%. The mean precipitation (\pm standard error) for these events is 3.32 mm \pm 0.59 mm. The mean amount of water intercepted per event (\pm standard error) is 0.09 mm \pm 0.03 mm.

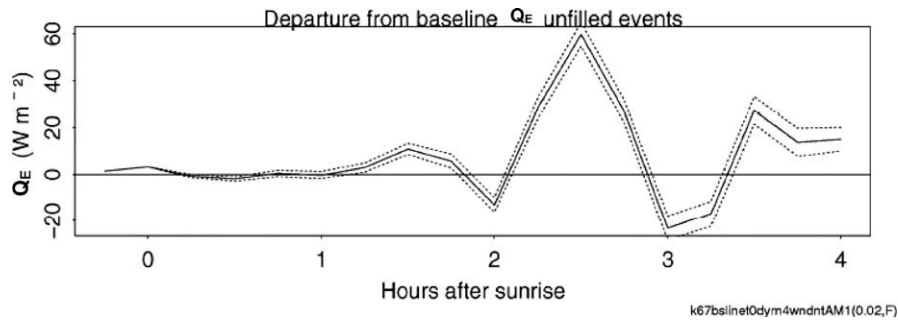


Fig. 12. Mean intercepted water binned by rainfall intensity for Penman-Monteith-filled daytime events, with the standard error bars for each rain intensity bin shown. The rain intensity bins are as follows: $\leq 2 \text{ mm h}^{-1}$, $2\text{--}7 \text{ mm h}^{-1}$, $7\text{--}16 \text{ mm h}^{-1}$, and $> 16 \text{ mm h}^{-1}$. The numbers along the bottom of the plot indicate the number of events included in each rain intensity bin.

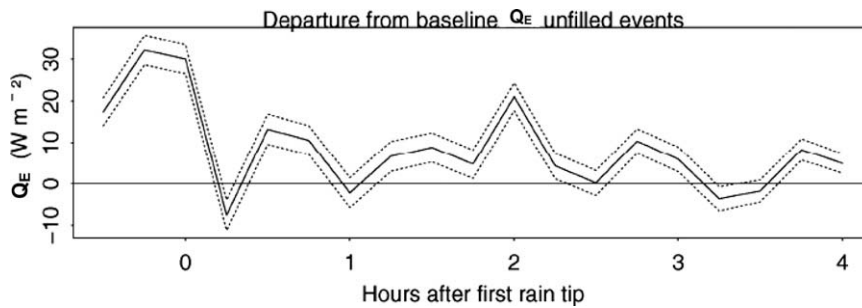


Fig. 13. Mean departure from baseline Q_E (W m^{-2}) for daytime rainfall events with rainfall intensities $\leq 16 \text{ mm h}^{-1}$ (solid black line, standard error dashed). A total of 104 events are included in the ensemble, and missing event data points were filled. The time $t = 0$ indicates the time of the first recorded tip by the rain gauge for tipping bucket rain gauge-recorded events or the first precipitation echoes detected by the ceilometer for ceilometer-detected events.

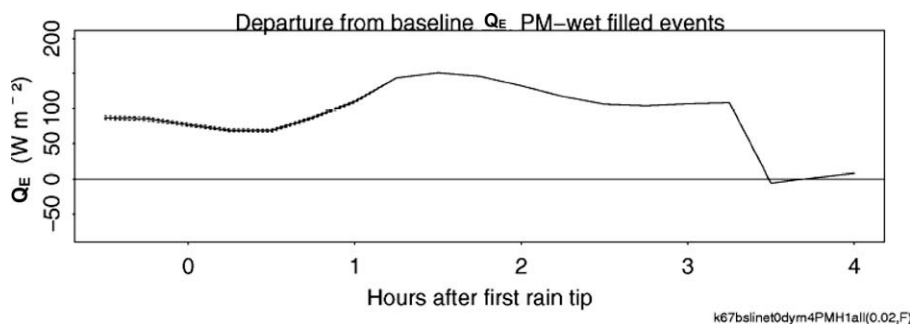


Fig. 14. Mean departure from baseline Q_E (W m^{-2}) for daytime Penman-Monteith-filled rainfall events with rainfall intensities $> 16 \text{ mm h}^{-1}$ (solid black line, standard error dashed). A total of 25 events are included in the ensemble, and missing event data points were not filled. The time $t = 0$ indicates the time of the first recorded tip by the rain gauge for tipping bucket rain gauge-recorded events or the first precipitation echoes detected by the ceilometer for ceilometer-detected events.

Daytime precipitation events

For daytime rainfall events, ensembles of departure from baseline Q_E (representing interception evaporation) were constructed for different classes of rainfall rates with respect to the rain-event starting times. At light-to-moderate rainfall rates for this site ($\leq 16 \text{ mm h}^{-1}$), there was a steady pulse of interception evaporation for 4 h following the event start (Fig. 13), with Q_E departure from baseline values maximizing at around 30 W m^{-2} approximately at the rain start time.

For the heavy rainfall-rate events ($> 16 \text{ mm h}^{-1}$), the Q_E departure ensemble from direct event Q_E observations indicated that the eddy-covariance system fails during the first hour after rainfall (not shown). For these events, the Penman-Monteith filled event Q_E was used to complete the ensemble Q_E (Fig. 14). The departure

from baseline Q_E was about 100 W m^{-2} during the first 3 h following rainfall, decreasing thereafter to near zero.

The mean intercepted water binned by rainfall intensity for daytime events (Fig. 15) shows an increase in the amount of water intercepted per event with increasing rainfall rate up to canopy capacity. The trend of the increase of intercepted water with rainfall rate is similar to that found by Murakami (2006); however the amount of intercepted water is much smaller in this study at the high-rainfall rates. This can be explained by the following reasons. First, rainfall rate in this study was reported as the average rainfall rate for an entire event. Second, the high-rainfall-rate events in our sample were all very short-duration convective showers that often occur in the afternoons in the dry season at the site. For the 25 high-rainfall-rate events in our dataset, the total duration of all events was 6.8 h, giving an average event duration of only about

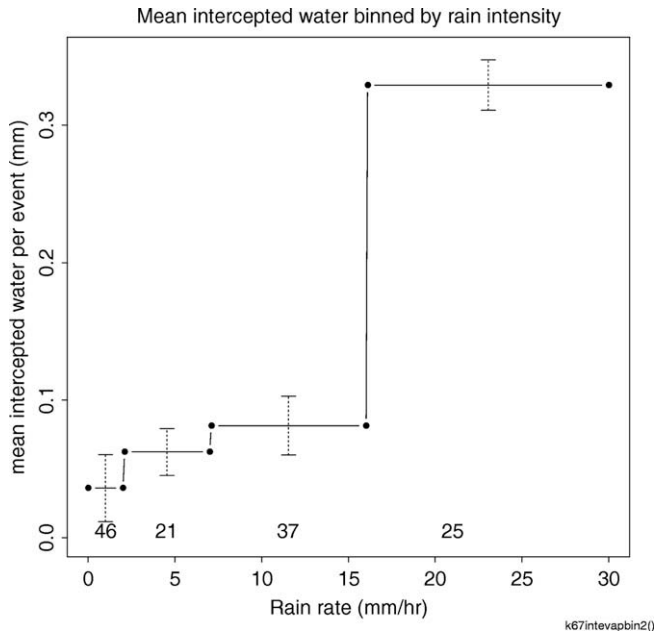


Fig. 15. Mean intercepted water binned by rainfall intensity for daytime events, with the standard error bars for each rain intensity bin shown. The rain intensity bins are as follows: $\leq 2 \text{ mm h}^{-1}$, $2\text{--}7 \text{ mm h}^{-1}$, $7\text{--}16 \text{ mm h}^{-1}$, and $>16 \text{ mm h}^{-1}$. The events in the $\leq 2 \text{ mm h}^{-1}$, $2\text{--}7 \text{ mm h}^{-1}$, and $7\text{--}16 \text{ mm h}^{-1}$ intensity bins used event Q_E , whereas the $>16 \text{ mm h}^{-1}$ bin used Penman-Monteith-filled Q_E . The numbers along the bottom of the plot indicate the number of events included in each rain intensity bin.

15-min. Had these events lasted for an hour, the amount of intercepted water measured would increase by a factor of four, and closer to the results of Murakami (2006).

The measurements from the events in the rainfall-rate bins less than 16 mm h^{-1} are directly from observations, with those from the $>16 \text{ mm h}^{-1}$ rainfall bin were estimated from the Penman-Monteith relation. A greater number of events at the high-rainfall rates would be needed to split the high-rainfall rate bin into smaller bins to determine whether the amount of intercepted water continues to increase towards a canopy capacity for rainfall rates $\geq 25 \text{ mm h}^{-1}$.

The mean intercepted water binned by rainfall intensity for daytime Penman-Monteith Q_E filled events showed a similar pattern to that found directly from observations, but with a slightly higher magnitude for the light-to-moderate rainfall-rate bins (not shown, see Czikowsky, 2009 for details).

The mean interception estimate for light rainfall-rate events ($\leq 2 \text{ mm h}^{-1}$) using observed event Q_E was 18% (Table 2), with estimates for moderate rainfall rates ($2\text{--}16 \text{ mm h}^{-1}$) decreasing to

about 10%. The percentage of daytime light-to-moderate rainfall events in our sample with good data (80.7%) is close to the percentage of all light-to-moderate rainfall events detected in our dataset (77.4%).

The mean interception estimates for light rainfall-rate events ($\leq 2 \text{ mm h}^{-1}$) and moderate rainfall rates ($2\text{--}16 \text{ mm h}^{-1}$) using Penman-Monteith filled event Q_E were 21.5% and 14.7%, respectively (Table 3), slightly higher from the corresponding observed values. Mean interception for the heavy rainfall events was 7.8%.

At the km67 study site, nearly half of the time rainfall rates are at the lightest category, with the heaviest rain rates only occurring about 6% of the time. However, due to the convective nature of the heavy precipitation, these heavy rainfall rates contribute one-third of the total rainfall amount at this site.

Dry and rain day energy-balance comparison

To compare the energy balance components for dry and rain days, ensembles of each of the components $-Q^*$, Q_E , and Q_H were assembled for dry days (189 days) and days with rain that started after 1400 GMT (100 days total). At the km67 site, the number of rainfall cases observed starts to increase in the late morning around 1400 GMT, with the greatest number of cases occurring at the afternoon convective peak. Choosing this time effectively separates the rainfalls associated with the nocturnal/early morning peak from the afternoon convective peak. Before 1200 GMT, $-Q^*$ for dry and rain days are close to each other. However, $-Q^*$ decreases on the rain days starting around 1200 GMT, about 2 h before the rain period on the rain days, representing increasing cloudiness (Fig. 16). For the remainder of the day, all of the energy balance components are greater in magnitude for the dry days than on the rain days.

Dividing the energy balance components for the dry and rain days by their respective $-Q^*$ values results in energy balance component fractions that can directly be compared for dry and rain days. When scaled by radiative energy, the effect of the rain on the energy balance components becomes more apparent (Fig. 17). During the early morning pre-rainfall period, the evaporative fraction is greater on the dry days than the rain days. Once the rainfall period is reached, the evaporative fraction becomes greater on the rain days than the dry days and remains so for the balance of the day. During the late afternoon period (1800–2200 GMT), the rain-day evaporative fraction is over 5% greater than the dry-day evaporative fraction (Table 4). On the rain days, the evaporative fraction increases over 16% from the pre-rain period to the late afternoon period, while the sensible heat fraction falls by 7%. Most of the energy required for the evaporative fraction increase on the rain days appears to be supplied by the storage term. From the pre-rainfall morning period to the late afternoon period, the storage fraction decreases by over 15%, falling to nega-

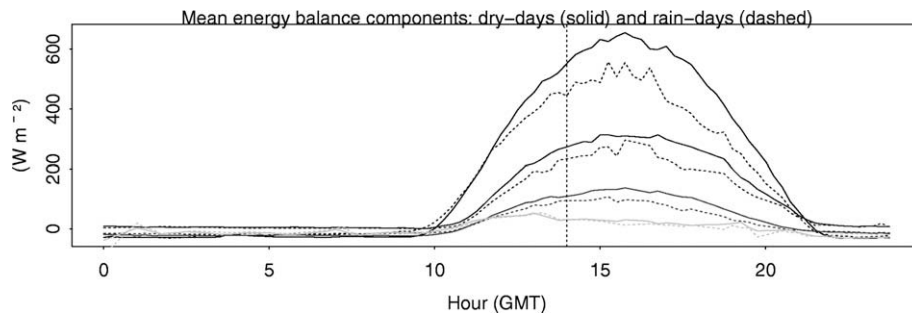


Fig. 16. Mean energy balance components for dry days (solid lines) and afternoon rain days (dashed lines). $-Q^*$ is shown in the top pair of lines, Q_E in the second pair of lines from top, Q_H in the third pair of lines from top, and Q_S in the bottom pair of lines. The dry-day ensemble includes 189 days, with 100 days in the rain-day ensemble. The vertical dashed line indicates the time (1400 GMT) after which rain fell during the rain days.

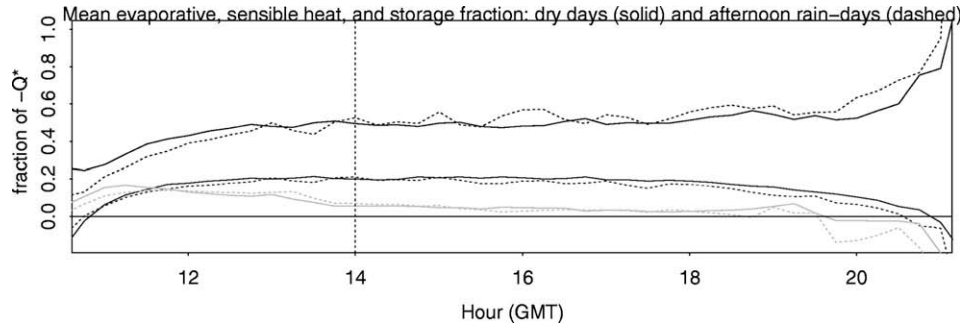


Fig. 17. Mean evaporative fraction (top pair of lines), sensible heat fraction (middle pair of lines), and storage fraction (bottom pair of lines) of $-Q^*$ for dry days (solid) and days with rain after 1400 GMT (dashed). The vertical dashed line indicates the 1400 GMT rain cutoff time. There are 189 days included in the dry-day ensemble and 100 days in the rain-day ensemble.

Table 4

Mean evaporative, sensible heat, and storage fractions of $-Q^*$ for dry and rain days for the pre-rain period 1200–1400 GMT and rain periods 1400–1800 GMT and 1800–2200 GMT.

(%)	1200–1400 GMT		1400–1800 GMT		1800–2200 GMT	
	Dry	Pre-rain	Dry	Rain	Dry	Rain
$[Q_E]/[-Q^*]$	47.5	44.4	49.3	51.8	55.5	60.7
$[Q_H]/[-Q^*]$	19.9	18.3	20.3	18.7	14.6	11.3
$[Q_S]/[-Q^*]$	10.2	11.8	4.3	4.3	0.0	–3.5

tive values indicating a release of energy. The storage fraction decrease nearly offsets the evaporative fraction increase on the rain days. Michiles and Gielow (2008) also reported negative storage fractions during rainfall, and concluded that storage is an important energy source for the evaporation of intercepted water by the forest canopy.

Bowen ratio (Q_H/Q_E) values during the pre-rainfall morning period are nearly the same for the dry and rain days (Fig. 18). Following the onset of rainfall, the rain-day Bowen ratio becomes lower than the dry-day Bowen ratio and remains so for the rest of the

day. For the period following rainfall (1400 GMT–2100 GMT), mean Bowen ratios for the dry and rain days are 0.34 and 0.28, respectively.

Summary

We introduce a methodology to directly observe the amount of interception evaporation using eddy-covariance data. We find interception from the difference of base state and rain event-based ensembles of observed latent heat flux. Mean interception for moderate daytime rainfall-rate events was about 10%, with light events at 18% and heavy events at 7.8%. The mean interception for all daytime and nocturnal events combined was 11.6%. This result is comparable to some recent interception studies in the Amazon where the spatial variation in throughfall was more adequately sampled (e.g., Ubarana, 1996; Lloyd and Marques, 1988; Tobón et al., 2000; Cuartas et al., 2007, Table 5). Larger departures from our result were found for other studies in the Amazon where the throughfall gauges were not moved (e.g., Franken et al., 1982a,b), or in tropical rain forest environments outside of the Amazon (Fig. 1).

An inherent advantage of using this method to estimate interception evaporation is that the footprint area of the eddy-covari-

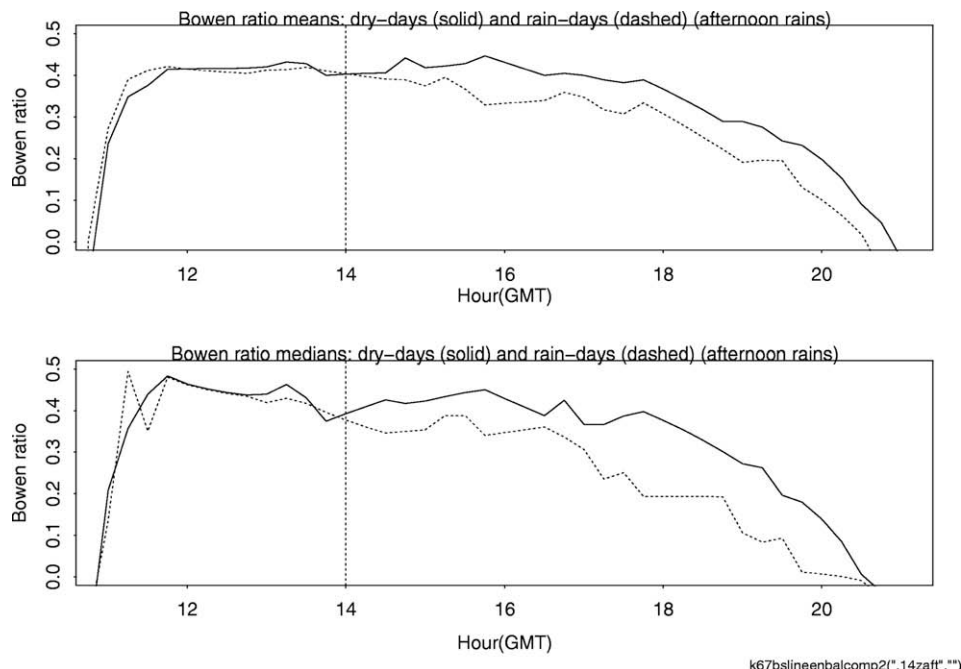


Fig. 18. Top: Mean Bowen ratio for dry days (solid line) and days with rain after 1400 GMT (dashed line). The vertical dashed line indicates the 1400 GMT rain cutoff time. Bottom: Same as top but Bowen ratio medians are plotted.

ance measurement incorporates the spatial variability in throughfall and interception that is a challenge to adequately sample using conventional methods, providing an average representative interception value over the entire flux footprint, and therefore be more suitable for catchment model input and validation. Furthermore, these estimates of interception evaporation represent additional information that can be extracted from standard eddy-covariance data already being collected, and until now have not been analyzed in this way.

We found that the bulk stomatal resistance does not vanish just after rainfall. Using the ensemble bulk stomatal resistances found during the dry and rainy days, we infer the wet canopy fraction during the rainfall events in this study to be about 40%. The ensemble bulk stomatal resistance for rainy days represents the average for saturated and partially wet canopies.

Evaporative fraction was approximately 15% higher on rain days than on dry days, with the energy being supplied by a nearly equivalent decrease in the canopy heat storage.

Tests of the method over an eastern Amazon old-growth rain forest show our method to be effective using direct observations under light-to-moderate rainfall rates ($\leq 16 \text{ mm h}^{-1}$). For events with heavy rainfall rates ($> 16 \text{ mm h}^{-1}$) when eddy covariance does not work, Penman-Monteith estimates of Q_E evaporation were used. To determine dry-day daytime base state ensembles, the method is applicable in nearly all daytime turbulent conditions. At night, base state latent heat flux is zero, so formation of base-state nocturnal ensembles is not necessary and the well-documented eddy covariance failures during calm, low-turbulent conditions are not applicable.

Acknowledgements

This work was supported as part of the LBA-ECO project, supported by the NASA Terrestrial Ecology Branch under Grants NCC5-283 and NNG-06GE09A (Phase 3 of LBA-ECO) to the authors' institution. We acknowledge the Harvard University group who ran instrumentation at the km67 site, and Lucy Hutyra and Elaine Gottlieb with providing information on the dataset and calibrations. We also acknowledge help in the field from Ricardo Sakai, Alex Tsoyref, Ralf Staebler, Otávio Acevedo, Osvaldo Moraes, Troy Beldini, Eleazar Brait, and Valderírio Miranda. We thank John Gash for his helpful review comments to improve the manuscript.

References

- Arcova, F., de Cicco, V., Rocha, P., 2003. Precipitação efetiva e interceptação das chuvas por floresta de Mata Atlântica em uma microbacia experimental em Cuhna-São Paulo. *R. Avore, Vicosa-MG* 27, pp. 257–262.
- Aylor, D.E., Ducharme, K.M., 1995. Wind fluctuations near the ground during rain. *Agricultural and Forest Meteorology* 76, 59–73.
- Baldocchi, D., Falge, E., Gu, L., Olson, R., Hollinger, D., Running, S., Anthoni, P., Bernhofer, C., Davis, K., Evans, R., Fuentes, J., Goldstein, A., Katul, G., Law, B., Lee, X., Malhi, Y., Meyers, T., Munger, W., Oechel, W., Paw, U.K.T., Pilegaard, K., Schmid, H.P., Valentini, R., Verma, S., Vesala, T., Wilson, K., Wofsy, S., 2001. Fluxnet: a new tool to study the temporal and spatial variability of ecosystem-scale carbon dioxide, water vapor, and energy flux densities. *Bulletin of the American Meteorological Society* 82, 2415–2434.
- Bouten, W., Swart, P.J.F., de Water, E., 1991. Microwave transmission, a new tool in forest hydrological research. *Journal of Hydrology* 124, 119–130.
- Brotzge, J.A., Duchon, C.E., 2000. A field comparison among a domeless net radiometer, two four-component net radiometers, and a domed net radiometer. *Journal of Atmospheric and Oceanic Technology* 17, 1569–1582.
- Cavelier, J., Jaramillo, M., Solis, D., de Leon, D., 1997. Water balance and nutrient inputs in bulk precipitation in tropical montane cloud forest in Panama. *Journal of Hydrology* 193, 83–96.
- Crockford, R.H., Richardson, D.P., 1990. Partitioning of rainfall in a eucalypt forest and pine plantation in south-eastern Australia: I. Effect of method and species composition. *Hydrological Processes* 4, 131–144.
- Cuartas, L.A., Tomasella, J., Nobre, A.D., Hodnett, M.G., Waterloo, M.J., Munera, J.C., 2007. Interception water-partitioning dynamics for a pristine rainforest in Central Amazonia: marked differences between normal and dry years. *Agricultural and Forest Meteorology* 145, 69–83.
- Czikowsky, M.J., 2009. Observations of the transient characteristics of the hydrological balance. Ph.D. Thesis, Department of Atmospheric and Environmental Sciences, University at Albany, State University of New York, 210 pp.
- Da Rocha, H.R., Goulden, M.L., Miller, S.D., Menton, M.C., Pinto, L.D.V.O., de Freitas, H.C., Figueira, A.M.S., 2004. Seasonality of water and heat fluxes over a tropical forest in eastern Amazonia. *Ecological Applications* 14, S22–S32.
- Dingman, S.L., 2002. *Physical Hydrology*, second ed. Prentice Hall, 646 pp.
- Eltahir, E.A.B., Bras, R.L., 1994. Precipitation recycling in the Amazon basin? *Quarterly Journal of the Royal Meteorological Society* 120, 861–880.
- Fernandes, K., Fu, R., Betts, A.K., 2008. How well does the ERA40 surface water budget compare to observations in the Amazon River basin. *Journal of Geophysical Research* 113, D11117. doi:10.1029/2007JD009220.
- Ferreira, S., Luizao, F., Dallarosa, R., 2005. Precipitação interna e interceptação da chuva em floresta de terra firme submetida a extração seletiva de madeira na Amazonia Central. *Acta Amazonica* 35, 55–62.
- Fitzjarrald, D.R., Acevedo, O.C., Moore, K.E., 2001. Climatic consequences of leaf presence in the eastern United States. *Journal of Climate* 14, 598–614.
- Fitzjarrald, D.R., Sakai, R.K., Moraes, O.L.L., Oliveira, R.C., Acevedo, O.C., Czikowsky, M.J., Beldini, T., 2008. Spatial and temporal rainfall variability near the Amazon Tapajós confluence. *Journal of Geophysical Research* 113, G00B11. doi:10.1029/2007JG000596.
- Franken, W., Leopoldo, R., Matsui, E., Ribeiro, M., 1982a. Interceptação das precipitações em floresta amazônica de terra firme. *Acta Amazonica* 12, 15–22.
- Franken, W., Leopoldo, P., Matsui, E., Ribeiro, M., 1982b. Estudo da interceptação da água de chuva em cobertura florestal amazônica do tipo terra firme. *Acta Amazonica* 12, 327–331.
- Gash, J.H.C., Lloyd, C.R., Lachaud, G., 1995. Estimating sparse forest rainfall interception with an analytical model. *Journal of Hydrology* 170, 79–86.
- Gash, J.H.C., Valente, F., David, J.S., 1999. Estimates and measurements of evaporation from wet, sparse pine forest in Portugal. *Agricultural and Forest Meteorology* 94, 149–158.
- Gash, J.H.C., 1979. An analytical model of rainfall interception by forests. *Quarterly Journal of the Royal Meteorological Society* 105, 43–55.
- Germer, S., Elsenbeer, H., Moraes, J., 2006. Throughfall and temporal trends of rainfall redistribution in an open tropical rainforest, SW Amazonia (Rodônia, Brazil). *Hydrology and Earth System Sciences* 10, 383–393.
- Grubb, P.J., 1977. Control of forest growth and distribution on wet tropical mountains: with special reference to mineral nutrition. *Annual Review of Ecology and Systematics* 8, 83–107.
- Herbst, M., Rosier, P.T.W., McNeil, D.D., Harding, R.J., Gowing, D.J., 2008. Seasonal variability of interception evaporation from the canopy of a mixed deciduous forest. *Agricultural and Forest Meteorology* 148, 1655–1667.
- Hewlett, J.D., 1982. *Principles of Forest Hydrology*. The University of Georgia Press, Athens, GA, 183 p.
- Holwerda, F., Scatena, F., Bruijnzeel, L., 2006. Throughfall in a Puerto Rican montane rainforest: a comparison of sampling strategies. *Journal of Hydrology* 327, 592–602.
- Huang, Y.S., Chen, S.S., Lin, T.P., 2005. Continuous monitoring of water loading of trees and canopy rainfall interception using the strain gauge method. *Journal of Hydrology* 311, 1–7.
- Hutyra, L.R., Munger, J.W., Nobre, C.A., Saleska, S.R., Vieira, S.A., Wofsy, S.C., 2005. Climatic variability and vegetation vulnerability in Amazonia. *Geophysical Research Letters* 32, L24712. doi:10.1029/2005GL024981.
- Imbach, A. et al., 1989. Modelling agroforestry systems of cacao (*Theobroma cacao*) with laurel (*Cordia alliodora*) and cacao with poro (*Erithrina poeppigiana*) in Costa Rica IV. Water balances. *Agroforestry Systems* 8, 267–287.
- Kaimal, J.C., Finnigan, J.J., 1994. *Atmospheric Boundary Layer Flows*. Oxford, 289 pp.
- Kimmins, J.P., 1973. Some statistical aspects of sampling throughfall precipitation in nutrient cycling studies in British Columbian coastal forests. *Ecology* 54, 1008–1019.
- Kume, T., Manfroi, O.J., Kuraji, K., Tanaka, N., Horiuchi, T., Suzuki, M., Kumagai, T., 2008. Estimation of canopy water storage capacity from sap flow measurements in a Bornean tropical rainforest. *Journal of Hydrology* 352, 288–295.
- Larsson, S., 1981. Influence of intercepted water on transpiration and evaporation of *Salix*. *Agricultural Meteorology* 23, 331–338.
- Lawrence, D.M., Thronton, P.E., Oleson, K.W., Bonan, G.B., 2007. The partitioning of evapotranspiration into transpiration, soil evaporation, and canopy evaporation in a GCM: impacts on land-atmosphere interaction. *Journal of Hydrometeorology* 8, 862–880.
- Leopoldo, P., Franken, W., Salati, E., Ribeiro, M., 1987. Towards a water balance in the Central Amazonian region. *Experientia* 43, 222–233.
- Lloyd, C.R., Marques, A.O., 1988. Spatial variability of throughfall and stemflow measurements in Amazonian forest. *Agricultural and Forest Meteorology* 42, 63–73.
- Lloyd, C.R., Gash, J.H.C., Shuttleworth, W.J., Marques, A.O., 1988. The measurement and modelling of rainfall interception by Amazonian rainforest. *Agricultural and Forest Meteorology* 43, 277–294.
- Lundberg, A., Eriksson, M., Halldin, S., Kellner, E., Seibert, J., 1997. New approach to the measurement of interception evaporation. *Journal of Atmospheric and Oceanic Technology* 14, 1023–1035.
- Manfroi, O. et al., 2006. Comparison of conventionally observed interception evaporation in a 100-m² subplot with that estimated in a 4-ha area of the same Bornean lowland tropical forest. *Journal of Hydrology* 329, 329–349.
- Massman, W.J., Lee, X., 2002. Eddy covariance flux corrections and uncertainties in long-term studies of carbon and energy exchanges. *Agricultural and Forest Meteorology* 113, 121–144.

- Michiles, A.A., Gielow, R., 2008. Above-ground thermal energy storage rates, trunk heat fluxes and surface energy balance in a central Amazonian rainforest. *Agricultural and Forest Meteorology* 148, 917–930.
- Mizutani, K., Ikeda, T., 1994. Evaporation of intercepted rainfall from a *Castanopsis cuspidata* Schottky forest using various micrometeorological methods. In: *Proceedings of the International Symposium on Forest Hydrology*, Tokyo, Japan, pp. 69–76.
- Mizutani, K., Yamanoi, K., Ikeda, T., Watanabe, T., 1997. Applicability of the eddy correlation method to measure sensible heat transfer to forest under rainfall conditions. *Agricultural and Forest Meteorology* 86, 193–203.
- Monteith, J.L., Unsworth, M.H., 1990. *Principles of Environmental Physics*. E. Arnold, 291 pp.
- Monteith, J. L., 1965. Evaporation and environment. In: *Symposia of the Society for Experimental Biology*, vol. 19, pp. 205–234.
- Moore, C.J., Fisch, G.F., 1986. Estimating heat storage in Amazonian tropical forest. *Agricultural and Forest Meteorology* 38, 147–168.
- Murakami, S., 2006. A proposal for a new forest canopy interception mechanism: splash droplet evaporation. *Journal of Hydrology* 319, 72–82.
- Muzylo, A., Llorens, P., Valente, F., Keizer, J.J., Domingo, F., Gash, J.H.C., 2009. A review of rainfall interception modelling. *Journal of Hydrology* 370, 191–206.
- Newson, M.D., Calder, I.R., 1989. Forests and water resources: problems of prediction on a regional scale. *Philosophical Transactions of the Royal Society of London B* 324, 283–298.
- Raupach, M.R., Finnigan, J.J., 1988. 'Single-layer models of evaporation from plant canopies are incorrect but useful, whereas multilayer models are correct but useless': discuss. *Australian Journal of Plant Physiology* 15, 705–716.
- Rogers, R.R., Lamoreux, M.F., Bissonnette, L.R., Peters, R.M., 1997. Quantitative interpretation of laser ceilometer intensity profiles. *Journal of Atmospheric and Oceanic Technology* 14, 396–411.
- Rutter, A.J., Kershaw, K.A., Robins, P.C., Morton, A.J., 1971. A predictive model of rainfall interception in forest. I. Derivation of the model from observations in a plantation of Corsican Pine. *Agricultural Meteorology* 9, 367–384.
- Rutter, A.J., Morton, A.J., Robins, P.C., 1975. A predictive model of rainfall interception in forest. II. Generalization of the model and comparison with observations in some coniferous and hardwood stands. *Journal of Applied Ecology* 12, 367–380.
- Sakai, R.K., Fitzjarrald, D.R., Moore, K.E., 2001. Importance of low-frequency contributions to eddy fluxes over rough surfaces. *Journal of Applied Meteorology* 40, 2178–2192.
- Salati, E., Vose, P.B., 1984. Amazon basin: a system in equilibrium. *Science* 225, 129–138.
- Saleska, S.R., Miller, S.D., Matross, D.M., Goulden, M.L., Wofsy, S.C., da Rocha, H.R., de Camargo, P.B., Crill, P., Daube, B.C., de Freitas, H.C., Hutyra, L., Keller, M., Kirchoff, V., Menton, M., Munger, J.W., Pyle, E.H., Rice, A.H., Silva, H., 2003. Carbon in Amazon forests: unexpected seasonal fluxes and disturbance-induced losses. *Science* 302, 1554–1557.
- Savenije, H.H.G., 2004. The importance of interception and why we should delete the term evapotranspiration from our vocabulary. *Hydrological Processes* 18, 1507–1511.
- Schubart, H., Franken, W., Luizao, F., 1984. Uma floresta sobre solos pobres. *Ciencia Hoje* 2, 26–32.
- Stewart, J.B., 1977. Evaporation from the wet canopy of a pine forest. *Water Resources Research* 13, 915–921.
- Tobón, C., Bouten, W., Sevnik, J., 2000. Gross rainfall and its partitioning into throughfall, stemflow, and evaporation of intercepted water in four Forest ecosystems in western Amazonia. *Journal of Hydrology* 237, 40–57.
- Ubarana, V., 1996. Observation and modelling of rainfall interception loss in two experimental sites in Amazonian forest. In: Gash, J., Nobre, C., Roberts, J., Victoria, R. (Eds.), *Amazonian Deforestation and Climate*. Chichester, New York, pp. 151–162.
- Van der Tol, C., Gash, J.H.C., Grant, S.J., McNein, D.D., Robinson, M., 2003. Average wet canopy evaporation for a Sitka spruce forest derived using the eddy correlation-energy balance technique. *Journal of Hydrology* 276, 12–19.
- Van Dijk, A., Meesters, A., Schellekens, J., Bruijnzeel, L., 2005. A two-parameter exponential rainfall depth-intensity distribution applied to runoff and erosion modeling. *Journal of Hydrology* 330, 155–171.
- Wallace, J., McJannet, D., 2006. On interception modelling of a lowland coastal rainforest in northern Queensland, Australia. *Journal of Hydrology* 329, 477–488.
- Zephoris, M., Holin, H., Lavie, F., Cenac, N., Cluzeau, M., Delas, O., Eideliman, F., Gagneux, J., Gander, A., Thibord, C., 2005. Ceilometer observations of aerosol layer structure above the Petit Luberon during ESCOMPTE's IOP 2. *Atmospheric Research* 74, 581–595.